Ionics (2019) 25:1315–1321
https://doi.org/10.1007/s11581-018-2759-0

ORIGINAL PAPER

Electrical properties of the ordered oxygen-deficient perovskite $Ca_2Fe_{0.5}Ga_{1.5}O_5$

Ram Krishna Hona[1] · Ashfia Huq[2] · Farshid Ramezanipour[1]

Received: 26 August 2018 / Revised: 28 September 2018 / Accepted: 5 October 2018 / Published online: 17 October 2018

Abstract

$Ca_2Fe_{0.5}Ga_{1.5}O_5$ is an oxygen-deficient perovskite, where the defects generated due to oxygen-deficiency are distributed in an ordered fashion. Neutron diffraction experiments indicate that the defect-order results in the formation of alternating $(Ga)O_4$ tetrahedral and $(FeGa)O_6$ octahedral units, forming the so-called brownmillerite-type structure. This material represents the highest degree of Ga-doping in the brownmillerite compound $Ca_2Fe_2O_5$, which can be achieved using solid-state synthesis method. X-ray photoelectron spectroscopy (XPS) combined with iodometric titration was employed to determine the Fe oxidation state and the oxygen-content in $Ca_2Fe_{0.5}Ga_{1.5}O_5$. The XPS studies show that Fe is predominantly in trivalent state, and the iodometric titrations indicate that the oxygen stoichiometry is 5.07 per formula unit, consistent with primarily trivalent Fe. Variable-temperature electrical conductivity studies of $Ca_2Fe_{0.5}Ga_{1.5}O_5$ have been performed in a wide temperature range, 25–800 °C, indicating semiconducting behavior and significant contribution of ionic conductivity to total conductivity of this material.

Keywords Electrical properties · Crystal structure · Ordering · Oxygen-deficient perovskite

Introduction

Many oxygen-deficient perovskite oxides exhibit mixed ionic-electronic conductivity [1]. Mixed conducting materials are important in different areas, such as gas sensing devices [2], electrodes for solid-oxide fuel cells [3], and electrocatalysts [4].

Oxygen deficient perovskites have general formula $ABO_{3-\delta}$, where δ represents the oxygen deficiency. The B-site cations usually form BO_6, BO_5, or BO_4 polyhedra depending on the structure, while the A-site cations reside in spaces between the polyhedra. The crystal structure can vary depending on different parameters including the magnitude of δ. For example, a series of structures have been observed for $SrMnO_{3-\delta}$ [5] and $Sr_2Fe_2O_{3-\delta}$ [6] due to the variation of oxygen stoichiometry. The crystal structure of oxygen-deficient perovskites also depends on the arrangement of defects that are generated due to oxygen-deficiency [7–11]. The defects can be distributed in a disordered [12–14] or ordered fashion [7–11, 15–19]. One of the common structures, resulting from the ordering of defects, is brownmillerite-type structure [7–11, 15–19]. In brownmillerite materials, the ordering of defects results in tetrahedral coordination geometry in alternating layers. As shown in Fig. 1, the BO_4 tetrahedra and BO_6 octahedra alternate in the crystal lattice. The tetrahedra form chains that run parallel to the octahedral layers. The orientation of tetrahedral chains with respect to each other can be different, leading to different space groups in brownmillerite compounds.

Changes in the A or B-site cations in oxygen-deficient perovskites, $ABO_{3-\delta}$, can change the crystal structure. One example is the significant difference between $Sr_2Fe_2O_5$, which has a brownmillerite-type structure, and $Ba_2Fe_2O_5$, that features a complex structure containing tetrahedral, square-pyramidal, and octahedral geometry [10]. The change in the crystal structure leads to significant differences in electrical properties of $Sr_2Fe_2O_5$ and $Ba_2Fe_2O_5$ [10]. Another example is the phase transitions in $La_{1-x}Sr_xFeO_{3-\delta}$ as a result of Sr-substitution on the A-site, leading to variation in physical properties [20]. The effect of the B-site cation is demonstrated by phase transitions in $SrFe_{1-x}Nb_xO_{3-\delta}$ ($x = 0.05$, 0.1, 0.2, 0.3, and 0.4) where an *I4/mmm* tetragonal structure transforms into a cubic

✉ Farshid Ramezanipour
farshid.ramezanipour@louisville.edu

[1] Department of Chemistry, University of Louisville, Louisville, KY 40292, USA

[2] Oak Ridge National Laboratory, Oak Ridge, TN 37931, USA

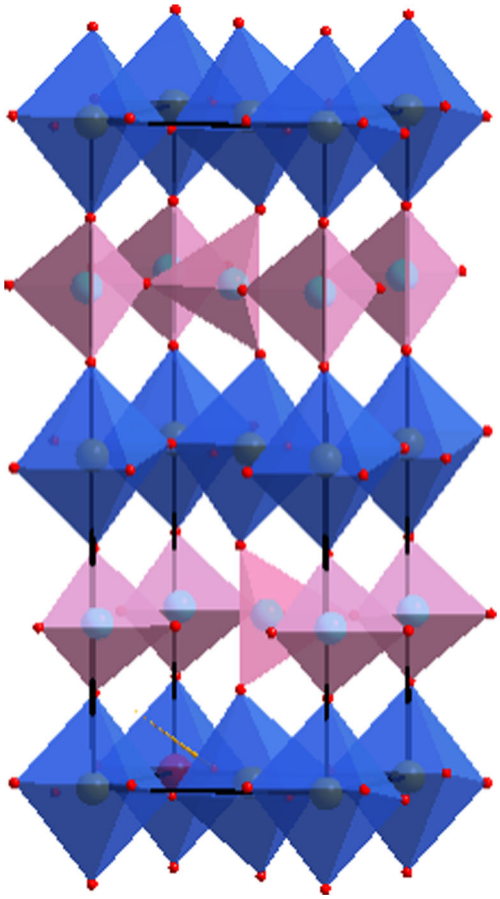

Fig. 1 Brownmillerite structure of $Ca_2Fe_{0.5}Ga_{1.5}O_5$

structure with *Pm*-3*m* space group [21]. The same study also reports a structural transition between cubic and orthorhombic due to the variation of the B-site cation [21].

Most oxygen-deficient perovskites contain transition metals on the B-site. However, main group metals, particularly those from group 13, can also be incorporated into these compounds, and occupy some of the B-sites [22–24]. Nevertheless, in most cases, the majority of cations on the B-site are still transition metal cations [22–24]. Brownmillerite materials, where the transition metals are eliminated from the structure, are interesting because they can exhibit predominantly ionic conductivity. Thus, they can be used in applications such as fuel cell electrolytes, where ionic conductivity is needed, but electronic conductivity is undesirable. One prominent example of a brownmillerite compound, which possesses only main group elements on the B-site, is the In-containing material $Ba_2In_2O_5$ [25] and its doped analogues [26, 27]. This material can be synthesized by solid-state method at high temperature [25]. However, the situation is different for Ga-only brownmillerite compounds, which seem to require high pressure to form [28]. For example, $Ca_2Ga_2O_5$ has been made under 2.5 GPa of pressure [28]. In addition, $Sr_2Ga_2O_5$ has been synthesized under 1.5 GPa of pressure, but this material does not form a brownmillerite structure [29].

There is one report on the crystal structure of $Ca_2Fe_{0.5}Ga_{1.5}O_5$, synthesized using standard solid-state synthesis method [28]. However, that study only reports the crystal structure using X-ray diffraction, and no other information regarding properties of $Ca_2Fe_{0.5}Ga_{1.5}O_5$ has been reported. In the current study, we have shown that $Ca_2Fe_{0.5}Ga_{1.5}O_5$ represents the maximum level of Ga-doping in $Ca_2Fe_2O_5$ system, which can be achieved by solid-state synthesis method. We have examined the Fe and Ga distribution using neutron diffraction, and have also studied electrical properties of this compound in a wide temperature range, 25–800 °C.

Materials and methods

Solid-state synthesis method was employed to prepare $Ca_2Fe_{0.5}Ga_{1.5}O_5$. The powders of the precursors $CaCO_3$ (Alfa Aesar, 99.95%), Fe_2O_3 (Alfa Aesar, 99.998%), and Ga_2O_3 (Sigma Aldrich, 99.99%) were mixed, pressed into a pellet, and heated at 1000 °C for 24 h in air. The samples were then reground and refired at 1200 °C for 24 h in air, followed by slow cooling. The heating and cooling rates were 100 °C/h. Synthesis of compositions containing higher Ga content was also attempted. However, single phase products could only be obtained at the maximum Ga concentration of 1.5 per formula unit. Iodometric titrations were performed under argon atmosphere, as described previously [10].

High resolution field-emission scanning electron microscopy (SEM) was used to study the micro-structure. X-ray photoelectron spectroscopy (XPS) was carried out at room temperature using Al Kα radiation (1486.7 eV). The electrical properties were investigated by direct-current (DC) and alternating-current (AC) on pellets that had been sintered at 1200 °C. The AC electrochemical impedance spectroscopy measurements were performed in the frequency range of 0.1 Hz to 1 MHz using a computer-controlled frequency response analyzer. The DC measurements were done by applying a constant voltage of 10 mV and collecting the output current. Variable-temperature electrical conductivity measurements were carried out during both heating and cooling cycles with 10 °C intervals. At each measurement temperature, enough time was given for conductivity equilibrium to be achieved before moving to the next temperature. Powder X-ray diffraction measurements were done at room temperature using Cu Kα1 radiation (λ = 1.54056 Å). Neutron diffraction experiments were performed on POWGEN diffractometer at Oak Ridge National Laboratory, with center wavelength of 0.7 Å. Rietveld refinements were done using GSAS software [30] and EXPEGUI interface [31].

Table 1 The refined structural parameters for $Ca_2Fe_{0.5}Ga_{1.5}O_5$ from neutron diffraction. Space group: *Pnma*, $a = 5.3669(2)$, $b = 14.6214(5)$, $c = 5.5927(2)$, $R_p = 0.0744$, $wR_p = 0.0479$

Elements	x	y	z	Multiplicity	Occupancy	U_{iso}
Ca	0.0076(6)	0.1075(1)	0.5281(3)	8	1	0.0013(2)
Ga1	0.0463(4)	0.25	0.0700(4)	4	1	0.0025(3)
Ga2	0.0	0.0	0.0	4	0.5	0.0004(2)
Fe	0.0	0.0	0.0	4	0.5	0.0004(2)
O1	0.3991(7)	0.25	0.1279(6)	4	1	0.0052(4)
O2	0.0193(5)	0.6412(2)	0.0710(4)	8	1	0.0063(3)
O3	0.2513(6)	0.0140(1)	0.2489(7)	8	1	0.0020(2)

Results and discussion

Crystal structure

As discussed in the experimental section, $Ca_2Fe_{0.5}Ga_{1.5}O_5$ represents the highest degree of Ga-doping in the brownmillerite compound, $Ca_2Fe_2O_5$, which can be achieved by solid-state synthesis method. Higher degree of Ga-doping is only possible if the synthesis is done in high pressure, 2.5 GPa [28]. The only report on $Ca_2Fe_{0.5}Ga_{1.5}O_5$ describes X-ray diffraction data of this material, indicating *Pcmn* space group [32]. Here, we study the structure using a combination of neutron and X-ray diffraction. The common space groups for brownmillerite compounds are *Imma*, *Ima*2, *Pnma* (*Pcmn*), and *Pbcm* [7, 8, 11, 16, 19].

The *Pbcm* space group is recognized by the presence of superstructure peaks, given that materials crystalizing in this space group have unit cells that are double the size of those for typical brownmillerites [7, 8, 11, 16, 19]. These superstructure peaks do not appear in the diffraction data for $Ca_2Fe_{0.5}Ga_{1.5}O_5$, ruling out the *Pbcm* space group. The *Pnma* space group is identified by the presence of the 131 peak, which is absent in I-centered space groups [7, 8, 11, 16, 19]. The powder X-ray and neutron diffraction data for $Ca_2Fe_{0.5}Ga_{1.5}O_5$ show the 131 peak, indicative of space group *Pnma*. This was then confirmed by Rietveld refinements. Table 1 lists the refined structural parameters, and Fig. 2 shows the X-ray and neutron refinement profiles. In these refinements, initially, Fe and Ga were mixed on both octahedral and tetrahedral sites. Refining the site-occupancies on these sites indicates that Fe is exclusively located on the octahedral site, while Ga occupies all of the tetrahedral sites and half of the octahedral positions.

Scanning electron microscopy data show high sinterability and good contact between crystallites of $Ca_2Fe_{0.5}Ga_{1.5}O_5$, as shown in Fig. 3. Oxidation state of Fe was investigated by X-ray photoelectron spectroscopy (XPS). The $2P_{3/2}$ peaks for trivalent and tetravalent Fe are expected to appear at ~710–711 eV [33, 34] and ~712–713 eV [35, 36], respectively. In addition, a satellite peak appearing at about 7–9 eV higher than the $2P_{3/2}$ peak is the signature of trivalent Fe [33, 34]. The XPS data for $Ca_2Fe_{0.5}Ga_{1.5}O_5$ (Fig. 4) show the $2P_{3/2}$ peak for Fe at ~710 eV followed by a satellite peak at ~718 eV, confirming that Fe is primarily in trivalent state. There is also a slight shoulder on the right side of the Fe $2P_{2/3}$ peak, which indicates the presence of a small amount of tetravalent Fe. These findings were then confirmed by iodometric titrations, which showed the accurate oxygen stoichiometry to be 5.07 mol per formula unit, i.e., $Ca_2Fe_{0.5}Ga_{1.5}O_{5.07}$. These results confirm the XPS findings that the oxidation state of Fe is primarily 3+, along with a small amount of tetravalent Fe.

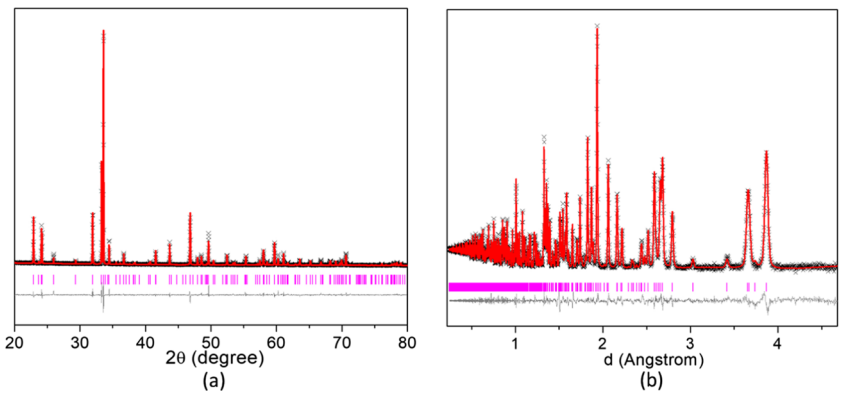

Fig. 2 Refinement profiles for $Ca_2Fe_{0.5}Ga_{1.5}O_5$ using **a** X-ray and **b** neutron diffraction

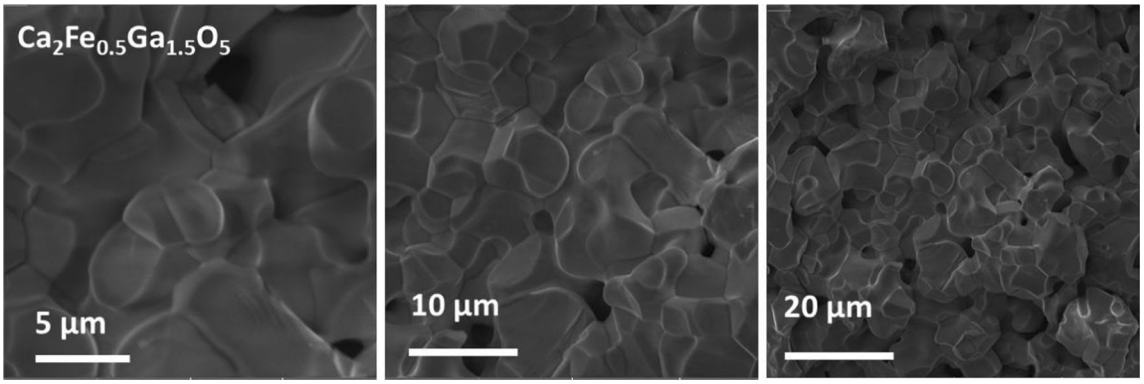

Fig. 3 SEM images of $Ca_2Fe_{0.5}Ga_{1.5}O_5$, showing good contact between the crystallites

Electrical properties

The electrical properties of $Ca_2Fe_{0.5}Ga_{1.5}O_5$ were studied by alternating current (AC) and direct current (DC) methods. In DC method, the output current (I) is measured while applying a constant voltage. This current is then converted into resistance using Ohm's law. In AC impedance spectroscopy, the resistance is determined from the intercept of the data with the real axis (Z′) of the Nyquist plot at low frequency. The resistance values (R) are then used to calculate the conductivity (σ) using the following equation:

$$\sigma = L/RA$$

where L and A represent the thickness and cross-sectional area of the sample, respectively. The electrical conductivity was also obtained at variable temperatures from 25 to 800 °C (Fig. 5). In brownmillerite compounds, the electronic conductivity is achieved due to the presence of cations that have multiple stable oxidation states such as $Fe^{2+}/Fe^{3+}/Fe^{4+}$. Variable oxidation states can also be created due to oxygen loss, i.e., partial reduction of cations, [37] or oxygen absorption, leading to partial oxidation [38, 39]. These processes result in the formation of small polarons [39]. The electrons hop through M^{m+}–O–M^{n+} conduction pathways, which are created due to the presence of variable oxidation states [40, 41]. However, many brownmillerite materials are mixed-conductors, where the total conductivity includes contribution from both electron and oxide-ion conductivity. The latter can become dominant when the transition metals are eliminated from the material composition [25].

In $Ca_2Fe_{0.5}Ga_{1.5}O_5$, contributions from both ionic and electronic conductivity are expected, considering the oxygen-vacancies and the presence of variable oxidation states of Fe in the material composition. The conductivity of $Ca_2Fe_{0.5}Ga_{1.5}O_5$, can be compared to a predominantly ionic conductor, $Ba_2In_2O_5$, which shows electrical conductivity values, that are less than ~ 10^{-3} Scm^{-1} at 700 °C [25]. Whereas the conductivity of $Ca_2Fe_{0.5}Ga_{1.5}O_5$ at the same temperature is more than one order of magnitude higher, ~ 10^{-2} Scm^{-1}. The higher conductivity of $Ca_2Fe_{0.5}Ga_{1.5}O_5$ may be attributed to the contribution of the electronic conductivity in addition to the ionic conductivity.

In oxide materials, the bulk, grain-boundary, and electrode-interface resistance can be determined using AC impedance spectroscopy. The observation of semicircles in the Nyquist plot of impedance spectroscopy indicates significant contribution from ionic conductivity, as described by other researchers [42]. The fit to the impedance data for $Ca_2Fe_{0.5}Ga_{1.5}O_5$ at 200 °C is shown in Fig. 6. Three resistance-capacitance (RC) units were used for this fit, where the RC unit at highest frequency (left) corresponds to the bulk resistance. The semicircle in the middle shows the grain-boundary resistance and the semicircle at the lowest frequency (right) represents the electrode interface resistance.

In some oxide materials, an increase in conductivity as a function of temperature is observed. This behavior is seen in $Ca_2Fe_{0.5}Ga_{1.5}O_5$. The temperature-dependent increase in electrical conductivity is expected, due to an increase in the mobility of charge carriers, [43] according to the following relation:

$$\sigma = ne\mu$$

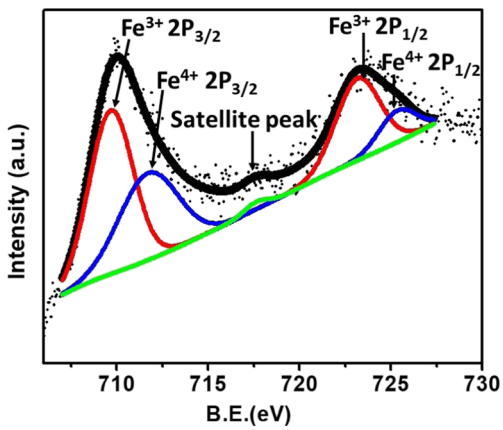

Fig. 4 X-ray photoelectron spectroscopy data for $Ca_2Fe_{0.5}Ga_{1.5}O_5$

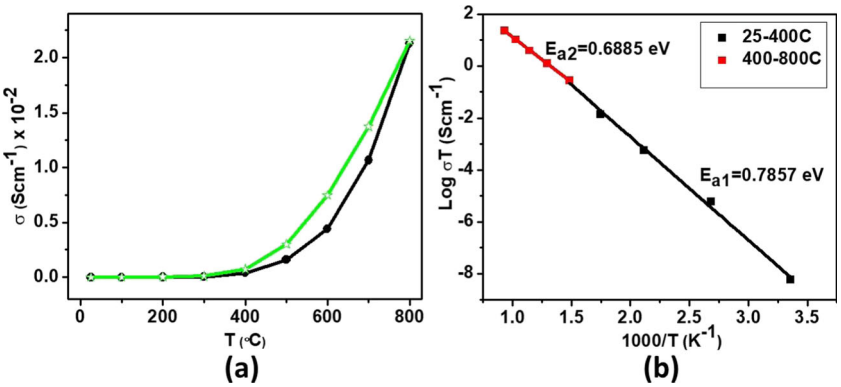

Fig. 5 **a** Electrical conductivity of $Ca_2Fe_{0.5}Ga_{1.5}O_5$ as a function of temperature. **b** Arrhenius plot and activation energies for $Ca_2Fe_{0.5}Ga_{1.5}O_5$

where σ, n, e, and μ are the conductivity, concentration of charge carriers, charge of electron, and mobility of the charge carriers, respectively. In addition, the loss of oxygen at higher temperature, as shown by thermogravimetric analysis (Fig. 7), can enhance the ionic conductivity, due to the increase in concentration of defects. It is known that oxide ion conductivity is enhanced above 500 °C [44, 45]. Fig. 5 shows a sharp increase in conductivity of $Ca_2Fe_{0.5}Ga_{1.5}O_5$ above 500 °C. We performed the variable-temperature conductivity measurements during both heating and cooling cycles. As noted in the experimental section, at each measurement temperature, enough time was given (~40 min) for the conductivity to plateau, i.e., equilibrate, before moving to the next temperature. An interesting observation is the presence of small hysteresis, where the conductivity values obtained during cooling have higher values than those obtained during heating. This behavior has been observed in some other materials before [46, 47]. Serval researchers have reported such hysteresis [46, 47], which have been attributed to oxygen-desorption [46], or defect-mediate ion mobility [47]. In $Ca_2Fe_{0.5}Ga_{1.5}O_5$, the hysteresis is very small, but it indicates the effect of oxide ion conductivity. As shown by TGA (Fig. 7), this material loses oxygen as temperature increases. The loss of oxygen can lead to enhanced ionic mobility, resulting in a small increase in total conductivity. The re-absorption of the lost oxygen upon cooling is a very slow process compared to the electronic transport phenomena. As a result, the enhanced ionic conductivity is retained after cooling the material, leading to hysteresis. It is noted that the hysteresis is observed at 500 °C and higher, where the contribution of ionic conductivity is expected to be more significant [44, 45].

We have also calculated the activation energies for the increase in electrical conductivity as a function of temperature. For thermally activated conductivity, activation energy can be calculated using the Arrhenius equation: [39, 48, 49].

$$\sigma T = \sigma^0 e^{\frac{-E_a}{KT}}$$

where σ^0 is a preexponential factor and a characteristic of the material. E_a, K, and T are the activation energy for the electrical conductivity, Boltzmann constant, and absolute temperature, respectively. The activation energy (E_a) is calculated from the slope of the line of best fit in the log σT versus $1000/T$ plot. The Arrhenius plot and activation energies for $Ca_2Fe_{0.5}Ga_{1.5}O_5$ are presented in Fig. 5, showing values close to those typically observed in this class of compounds.

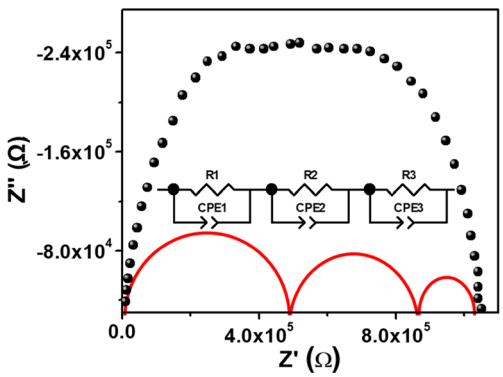

Fig. 6 AC impedance data for $Ca_2Fe_{0.5}Ga_{1.5}O_5$ at 200 °C. Three resistance-capacitance units indicate the bulk (left), grain boundary (middle), and electrode interface (right) resistance

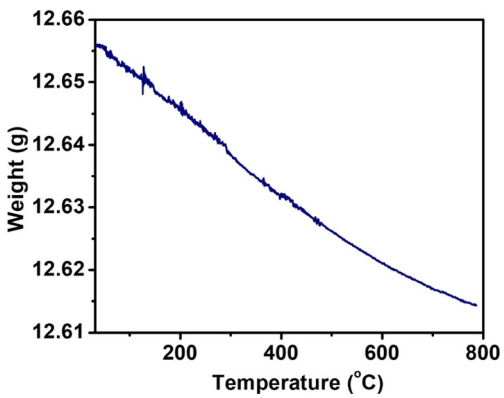

Fig. 7 Thermogravimetric analysis for $Ca_2Fe_{0.5}Ga_{1.5}O_5$

Conclusions

$Ca_2Fe_{0.5}Ga_{1.5}O_5$ represents the highest degree of Ga-doping in the brownmillerite compound, $Ca_2Fe_2O_5$, which can be reached through solid-state synthesis method. The distribution of Fe and Ga in this material has been determined by neutron diffraction. The electrical conductivity of $Ca_2Fe_{0.5}Ga_{1.5}O_5$ indicates semiconducting behavior, and mixed ionic-electronic conductivity. The results from XPS and iodometric titrations for $Ca_2Fe_{0.5}Ga_{1.5}O_5$ are consistent, and indicate that Fe is primarily in trivalent state, accompanied by a small amount of tetravalent Fe.

Acknowledgements F.R. thanks the Conn Center for Renewable Energy Research and Jacek Jasinski for their help. A portion of this research used resources at the Spallation Neutron Source, a DOE Office of Science User Facility operated by the Oak Ridge National Laboratory.

Funding information This work is supported in part by the National Science Foundation under Cooperative Agreement No. 1355438.

Compliance with ethical standards

Conflict of interest The authors declare no conflict of interest.

References

1. Patrakeev MV, Kharton VV, Bakhteeva YA, Shaula AL, Leonidov IA, Kozhevnikov VL, Naumovich EN, Yaremchenko AA, Marques FMB (2006) Oxygen nonstoichiometry and mixed conductivity of $SrFe_{1-x}M_xO_{3-\delta}$ (M=Al, Ga): effects of B-site doping. Solid State Sci 8(5):476–487. https://doi.org/10.1016/j.solidstatesciences.2006.01.006
2. Gómez L, Galeano V, Parra R, Michel CR, Paucar C, Morán O (2015) Carbon dioxide gas sensing properties of ordered oxygen deficient perovskite $LnBaCo_2O_{5+\delta}$ (Ln=La, Eu). Sensors Actuators B: Chem 221:1455–1460. https://doi.org/10.1016/j.snb.2015.07.080
3. Liu P, Luo Z, Kong J, Yang X, Liu Q, Xu H (2018) $Ba_{0.5}Sr_{0.5}Co_{0.8}Fe_{0.2}O_{3-\delta}$-based dual-gradient cathodes for solid oxide fuel cells. Ceram Int 44(4):4516–4519. https://doi.org/10.1016/j.ceramint.2017.12.034
4. Chen G, Zhou W, Guan D, Sunarso J, Zhu Y, Hu X, Zhang W, Shao Z (2017) Two orders of magnitude enhancement in oxygen evolution reactivity on amorphous $Ba_{(0.5)}Sr_{(0.5)}co_{(0.8)}Fe_{(0.2)}O_{(3-\delta)}$ nanofilms with tunable oxidation state. Sci Adv 3(6):e1603206. https://doi.org/10.1126/sciadv.1603206
5. Suescun L, Chmaissem O, Mais J, Dabrowski B, Jorgensen JD (2007) Crystal structures, charge and oxygen-vacancy ordering in oxygen deficient perovskites $SrMnO_x$ (x<2.7). J Solid State Chem 180(5):1698–1707. https://doi.org/10.1016/j.jssc.2007.03.020
6. Hodges JP, Jorgensen JD, Xiong X, Dabrowski B, Mini SM, Kimball CW, Materials Science D, Northern Illinois U (2000) Evolution of oxygen-vacancy ordered crystal structures in the perovskite series $Sr_nFe_nO_{3n-1}$ (n=2, 4, 8, and ∞), and the relationship to electronic and magnetic properties. J Solid State Chem 151(190):209. https://doi.org/10.1006/jssc.1999.8640
7. Hona RK, Huq A, Mulmi S, Ramezanipour F (2017) Transformation of structure, electrical conductivity, and magnetism in $AA'Fe_2O_{6-\delta}$, a = Sr, ca and a′ = Sr. Inorg Chem 56(16):9716–9724. https://doi.org/10.1021/acs.inorgchem.7b01228
8. Hona RK, Huq A, Ramezanipour F (2017) Unraveling the role of structural order in the transformation of electrical conductivity in $Ca_2FeCoO_{6-\delta}$, $CaSrFeCoO_{6-\delta}$, and $Sr_2FeCoO_{6-\delta}$. Inorg Chem 56(23):14494–14505. https://doi.org/10.1021/acs.inorgchem.7b02079
9. Mulmi S, Hona RK, Jasinski JB, Ramezanipour F (2018) Electrical conductivity of $Sr_{2-x}Ca_xFeMnO_5$ (x = 0, 1, 2). J Solid State Electrochem 22:2329–2338. https://doi.org/10.1007/s10008-018-3947-6
10. Hona RK, Ramezanipour F (2018) Variation in electrical conductivity of $A_2 Fe_2 O_5$ (A = Sr, Ba): the role of structural order. Mater Res Express 5(7):076307
11. Ramezanipour F, Greedan JE, Cranswick LMD, Garlea VO, Donaberger RL, Siewenie J (2012) Systematic study of compositional and synthetic control of vacancy and magnetic ordering in oxygen-deficient perovskites $Ca_2Fe_{2-x}Mn_xO_{5+y}$and $CaSrFe_{2-x}Mn_xO_{5+y}$ (x = 1/2, 2/3, and 1; y = 0–1/2). J Am Chem Soc 134(6):3215–3227. https://doi.org/10.1021/ja210985t
12. Hona RK, Ramezanipour F (2018) Disparity in electrical and magnetic properties of isostructural oxygen-deficient perovskites $BaSrCo_2O_{6-\delta}$ and $BaSrCoFeO_{6-\delta}$. J Mater Sci Mater Electron 29:13464–13473. https://doi.org/10.1007/s10854-018-9471-8
13. Ramezanipour F, Greedan JE, Siewenie J, Proffen T, Ryan DH, Grosvenor AP, Donaberger RL (2011) Local and average structures and magnetic properties of Sr_2FeMnO_{5+y}, y = 0.0, 0.5. Comparisons with Ca_2FeMnO_5 and the effect of the A-site cation. Inorg Chem 50(16):7779–7791. https://doi.org/10.1021/ic200919m
14. Ramezanipour F, Greedan JE, Siewenie J, Donaberger RL, Turner S, Botton GA (2012) A vacancy-disordered, oxygen-deficient perovskite with long-range magnetic ordering: local and average structures and magnetic properties of $Sr_2Fe_{1.5}Cr_{0.5}O_5$. Inorg Chem 51(4):2638–2644. https://doi.org/10.1021/ic202590r
15. Hona RK, Huq A, Ramezanipour F (2018) Magnetic structure of $CaSrFeCoO_{6-\delta}$: correlations with structural order. Mater Res Bull 106:131–136. https://doi.org/10.1016/j.materresbull.2018.05.030
16. Ramezanipour F, Greedan JE, Grosvenor AP, Britten JF, Cranswick LMD, Garlea VO (2010) Intralayer cation ordering in a brownmillerite superstructure: synthesis, crystal, and magnetic structures of Ca_2FeCoO_5. Chem Mater 22(21):6008–6020. https://doi.org/10.1021/cm1023025
17. Turner S, Verbeeck J, Ramezanipour F, Greedan JE, Van Tendeloo G, Botton GA (2012) Atomic resolution coordination mapping in Ca_2FeCoO_5 brownmillerite by spatially resolved electron energy-loss spectroscopy. Chem Mater 24(10):1904–1909. https://doi.org/10.1021/cm300640g
18. Ramezanipour F, Greedan JE, Cranswick LMD, Garlea VO, Siewenie J, King G, Llobet A, Donaberger RL (2012) The effect of the B-site cation and oxygen stoichiometry on the local and average crystal and magnetic structures of $Sr_2Fe_{1.9}M_{0.1}O_{5+y}$ (M = Mn, Cr, Co; y = 0, 0.5). J Mater Chem 22(19):9522–9538. https://doi.org/10.1039/C2JM30957B
19. Ramezanipour F, Cowie B, Derakhshan S, Greedan JE, Cranswick LMD (2009) Crystal and magnetic structures of the brownmillerite compound $Ca_2Fe_{1.039(8)}Mn_{0.962(8)}O_5$. J Solid State Chem 182(1):153–159. https://doi.org/10.1016/j.jssc.2008.10.010
20. Fossdal A, Menon M, Wærnhus I, Wiik K, Einarsrud MA, Grande T (2005) Crystal structure and thermal expansion of $La_{1-x}Sr_xFeO_{3-\delta}$ materials. J Am CeramSoc 87(10):1952–1958. https://doi.org/10.1111/j.1151-2916.2004.tb06346.x
21. Anikina PV, Markov AA, Patrakeev MV, Leonidov IA, Kozhevnikov VL (2009) The structure, nonstoichiometry, and thermodynamic characteristics of oxygen in strontium ferrite doped

with niobium, $SrFe_{1-x}Nb_xO_{3-\delta}$. Russ J Phys Chem A 83(5):699–704. https://doi.org/10.1134/S0036024409050021
22. Colville AA, Geller S (1971) The crystal structure of brownmillerite, Ca_2FeAlO_5. Acta Cryst B27:2311
23. D'Hondt H, Hadermann J, Abakumov AM, Kalyuzhnaya AS, Rozova MG, Tsirlin AA, Nath R, HaiyanTan JV, Antipov EV, Van Tendeloo G (2009) Synthesis, crystal structure and magnetic properties of the $Sr_2Al_{0.78}Mn_{1.22}O_{5.2}$ anion-deficient layered perovskite. J Solid State Chem 182:356–363
24. Lindberg F, Istomin SY, Berastegui P, Svensson G, Kazakov SM, Antipov EV (2003) Synthesis and structural studies of $Sr_2Co_{2-x}Ga_xO_5$, $0.3 \leqslant x \leqslant 0.8$. J Solid State Chem 173(2):395–406. https://doi.org/10.1016/S0022-4596(03)00129-4
25. Zhang GB, Smyth DM (1995) Defects and transport of the brownmillerite oxides with high oxygen ion conductivity — $Ba_2In_2O_5$. Solid State Ionics 82(3):161–172. https://doi.org/10.1016/0167-2738(95)00196-2
26. Didier C, Claridge J, Rosseinsky M (2014) Crystal structure of brownmillerite Ba_2InGaO_5. J Solid State Chem 218:38–43. https://doi.org/10.1016/j.jssc.2014.06.011
27. Mohn CE, Allan NL, Stølen S (2006) Sr and Ga substituted $Ba_2In_2O_5$: linking ionic conductivity and the potential energy surface. Solid State Ionics 177(3):223–228. https://doi.org/10.1016/j.ssi.2005.11.006
28. Kahlenberg V, Shaw CSJ (2001) Ca2Ga2O5: a new high pressure oxogallate. Z Kristallog - Cryst Mater 216(4):206–209
29. Kahlenberg V, Goettgens V, Mair P, Schmidmair D (2015) High-pressure synthesis and crystal structures of the strontium oxogallates $Sr_2Ga_2O_5$ and $Sr_5Ga_6O_{14}$. J Solid State Chem 228:27–35. https://doi.org/10.1016/j.jssc.2015.04.016
30. Larson AC, Von Dreele RB (2000) General structure analysis system (GSAS). Los Alamos National Laboratory Report LAUR:86–748
31. Toby BH (2001) A graphical user interface for GSAS. J Appl Crystallogr 34:210–213
32. Luo K, Amano Patino M, Hayward MA (2015) $Ca_2Cr_{0.5}Ga_{1.5}O_5$—an extremely redox-stable brownmillerite phase. J Solid State Chem 222:71–75. https://doi.org/10.1016/j.jssc.2014.11.011
33. Julián Morales LS, Martín F, Berry F, Renc X (2005) Synthesis and characterization of nanometric Iron and Iron-titanium oxides by mechanical milling: electrochemical properties as anodic materials in Lithium cells. J Electrochem Soc 152(9):A1748–A1754
34. Doi A, Nomura M, Obukuro Y, Maeda R, Obata K, Matsushima S, Kobayashi K (2014) Characterization of Ti-doped $CaFe_2O_4$ prepared from a malic acid complex. J Ceram Soc Jpn 122(2):175–178
35. Ruttanapun C, Maensiri S (2015) Effects of spin entropy and lattice strain from mixed-trivalent Fe^{3+}/Cr^{3+} on the electronic, thermoelectric and optical properties of delafossite $CuFe_{1-x}Cr_xO_2$ (x = 0.25, 0.5, 0.75). J Phys D Appl Phys 48:495103. https://doi.org/10.1088/0022-3727/48/49/495103
36. Ghaffari M, Liu T, Huang H, Tan OK, Shannon M (2012) Investigation of local structure effect and X-ray absorption characteristics (EXAFS) of Fe (Ti) K-edge on photocatalyst properties of $SrTi_{(1-x)}Fe_xO_{(3-\delta)}$. Mater Chem Phys 136(2):347–357. https://doi.org/10.1016/j.matchemphys.2012.06.037
37. Mueller DN, De Souza RA, Yoo H-I, Martin M (2012) Phase stability and oxygen nonstoichiometry of highly oxygen-deficient perovskite-type oxides: a case study of $(Ba,Sr)(Co,Fe)O_{3-\delta}$. Chem Mater 24(2):269–274. https://doi.org/10.1021/cm2033004
38. Shaula A, Pivak Y, Waerenborgh J, Gaczynski P, Yaremchenko A, Kharton V (2006) Ionic conductivity of brownmillerite-type calcium ferrite under oxidizing conditions. Solid State Ionics 177(33–34):2923–2930. https://doi.org/10.1016/j.ssi.2006.08.030
39. Asenath-Smith E, Lokuhewa IN, Misture ST, Edwards DD (2010) p-Type thermoelectric properties of the oxygen-deficient perovskite $Ca_2Fe_2O_5$ in the brownmillerite structure. J Solid State Chem 183(7):1670–1677. https://doi.org/10.1016/j.jssc.2010.05.016
40. Zhang Q, Xu ZF, Wang LF, Gao SH, Yuan SJ (2015) Structural and electromagnetic properties driven by oxygen vacancy in $Sr_2FeMoO_{6-\delta}$ double perovskite. J Alloys Compd 649:1151–1155. https://doi.org/10.1016/j.jallcom.2015.07.211
41. Kozhevnikov VL, Leonidov IA, Mitberg EB, Patrakeev MV, Petrov AN, Poeppelmeier KR (2003) Conductivity and carrier traps in $La_{1-x}SrxCo_{1-z}Mn_zO_{3-\delta}$ (x=0.3; z=0 and 0.25). J Solid State Chem 172(2):296–304. https://doi.org/10.1016/S0022-4596(03)00088-4
42. Kontoulis I, Steele BCH (1992) Fabrication and conductivity of a new compound $Ca_2Cr_2O_5$. J Eur Ceram Soc 9:459–462
43. Asenath-Smith E, Misture ST, Edwards DD (2011) Structural behavior and thermoelectric properties of the brownmillerite system $Ca_2(ZnxFe_{2-x})O_5$. J Solid State Chem 184(8):2167–2177. https://doi.org/10.1016/j.jssc.2011.06.009
44. Bhosale DR, Yusuf SM, Kumar A, Mukadam MD, Patil SI (2017) High oxide ion conductivity below 500 °C in garnets $La_xY_{3-x}Fe_5O_{12+\delta}$. Phys Rev Mater 1(1):015001. https://doi.org/10.1103/PhysRevMaterials.1.015001
45. Corallini S, Ceretti M, Cousson A, Ritter C, Longhin M, Papet P, Paulus W (2017) Cubic Sr^2ScGaO^5 perovskite: structural stability, oxygen defect structure, and ion conductivity explored on single crystals. Inorg Chem 56(5):2977–2984. https://doi.org/10.1021/acs.inorgchem.6b03106
46. Fargali AA, Zayed MK, Khedr MH, Moustafa AF (2008) Phase and conductivity dynamics of strontium hexaferrite nanocrystals in a hydrogen gas flow. Int J Phys Sci 3:131–139
47. Richardson G, O'Kane SEJ, Niemann RG, Peltola TA, Foster JM, Cameron PJ, Walker AB (2016) Can slow-moving ions explain hysteresis in the current–voltage curves of perovskite solar cells? Energy Environ Sci 9(4):1476–1485. https://doi.org/10.1039/C5EE02740C
48. Andoulsi R, Horchani-Naifer K, Férid M (2013) Electrical conductivity of $La_{1-x}Ca_xFeO_{3-\delta}$ solid solutions. Ceram Int 39(6):6527–6531. https://doi.org/10.1016/j.ceramint.2013.01.085
49. Pizzini S (2015) Physical chemistry of semiconductor materials and Processes. Wiley, West Sussex